Reliable Determination of Electron Diffusion Length and Charge Separation Efficiency in Dye-Sensitized Solar Cells

ARTICLE *in* THE JOURNAL OF PHYSICAL CHEMISTRY C · AUGUST 2010

Impact Factor: 4.77 · DOI: 10.1021/jp105486k

3 AUTHORS:

James Robert Jennings
Universiti Brunei Darussalam
37 PUBLICATIONS **1,466** CITATIONS
SEE PROFILE

Feng Li
Australian Centre for Advanced Photovolta…
7 PUBLICATIONS **182** CITATIONS
SEE PROFILE

Qing Wang
University of Reading
78 PUBLICATIONS **3,839** CITATIONS
SEE PROFILE

Reliable Determination of Electron Diffusion Length and Charge Separation Efficiency in Dye-Sensitized Solar Cells

James R. Jennings, Feng Li, and Qing Wang*

Department of Materials Science and Engineering, Nanocore, National University of Singapore, Singapore 117574

Received: June 15, 2010; Revised Manuscript Received: July 20, 2010

Reliable quantification of parameters influencing the efficiency of dye-sensitized solar cells (DSCs) is essential to guide device optimization and improve the fundamental understanding of device operation. The small-perturbation electron diffusion length (L_n) in DSCs has been determined by electrochemical impedance spectroscopy and by analysis of incident photon-to-collected-electron conversion efficiency (IPCE) spectra. When measurement conditions are chosen so that recombination can be treated as first-order in the free electron concentration, L_n values obtained by the two quite different techniques are found to be in good agreement. This result provides an important experimental validation of the simple diffusion−recombination model that is commonly used to explain DSC operation. Knowledge of L_n facilitates deconvolution of the charge separation efficiency (η_{sep}) from IPCE. η_{sep} is found to decrease significantly with increasing V_{OC} for all DSCs studied here. This phenomenon is likely to be caused by a decrease in sensitizer regeneration efficiency as electrons accumulate in the TiO_2, and sensitizer regeneration by iodide can no longer effectively compete with electron transfer from the TiO_2 to the oxidized sensitizer.

Introduction

Dye-sensitized solar cells (DSCs)[1] continue to attract a great deal of attention as a potentially low-cost alternative to conventional silicon-based photovoltaic technologies. Certified power conversion efficiencies in excess of 11% have been reported for small-area laboratory test devices,[2] whereas large-scale modules are reported to have achieved efficiencies of up to 8.4%.[3] To guide the optimization of DSCs, it is essential that the different factors governing the power conversion efficiency of devices are well-understood and can be reliably quantified. One such device parameter is the electron diffusion length (L_n), which can be defined as the average distance an electron travels before it is lost to recombination.[4] For the case where the recombination rate scales linearly with electron concentration, L_n is a constant device parameter and can be used to predict the charge collection efficiency (η_{col}) for a given spatial photogeneration rate profile.[5−7]

Several recent studies have indicated that values of L_n derived by different methodological approaches can be significantly different; values have been found to disagree by as much as a factor of 2−3.[5,7−10] It has been shown that the reason for the discrepancy between techniques is probably caused by an invalid assumption in the analysis of steady-state data, namely, that recombination of electrons with electrolyte species is first-order in conduction band (or free) electron concentration.[4,10] Nonlinear recombination kinetics in dye-sensitized solar cells has two important implications with respect to L_n. First, and most importantly, the concept of diffusion length is no longer particularly useful as it must depend upon the particular electron concentration profile in the TiO_2 layer. Second, L_n, which can be obtained from small-perturbation measurements (e.g., electrochemical impedance spectroscopy), is predicted to vary with electron concentration, as has been observed experimentally in several studies.[10,11]

Despite the limited relevance of L_n obtained by small-perturbation methods to actual device operation, it remains important to reaffirm the underlying theoretical models commonly used to describe DSCs by testing whether L_n values derived by steady-state and dynamic techniques are in agreement under conditions where the assumptions made in both analyses should be valid. In a related study, Leng et al. have recently found that steady-state IPCE measurements and transient photovoltage measurements yield similar values of L_n in a TiO_2-based water-splitting cell. L_n is also found to be approximately independent of bias voltage and, hence, electron concentration.[12] These authors suggest that the agreement between techniques arises because the assumption of linear recombination dynamics, implied by a constant L_n, is justified for this system. For the case of DSCs, no study to date has demonstrated a direct correspondence between L_n values derived by different methodological approaches.

In this article, we show that L_n determined by analysis of incident photon-to-collected-electron conversion efficiency (IPCE) spectra is in good agreement with L_n determined by electrochemical impedance spectroscopy (EIS), provided care is taken to ensure that assumptions made in data analysis are valid. We go on to demonstrate that knowledge of L_n, combined with IPCE spectra and optical characterization, can provide useful information regarding charge separation efficiency (η_{sep}) in these cells. To do this, we have measured IPCE spectra using low-intensity probe illumination, with DSCs biased close to open-circuit and under background illumination from bright, but relatively weakly absorbed, illumination ($\lambda = 627$ nm). These conditions ensure an almost position-independent electron concentration in the TiO_2 layer and permit linearization of the commonly used free electron continuity equation so that existing approaches used to determine L_n from IPCE spectra remain valid, even in the presence of nonlinear recombination.

For comparison with results obtained by analysis of IPCE spectra, we have chosen to use EIS for the independent determination of L_n, instead of combined measurements of

* To whom correspondence should be addressed. E-mail: qing.wang@nus.edu.sg.

10.1021/jp105486k
Published on Web 08/05/2010

charge density and transport/recombination time constants as used by some other authors. This is because intensity-modulated photocurrent spectroscopy[13] or transient photocurrent experiments used to obtain transport time constants (and ultimately electron diffusion coefficients) are typically performed under short-circuit conditions. At short-circuit, the free electron concentration in the TiO_2 layer is expected to be position-dependent due to electron extraction at the anode.[14,15] The influence of multiple trapping and nonlinear recombination on the time constants obtained from dynamic experiments performed under short-circuit conditions has not yet been unambiguously determined, although this point has been discussed before.[7,9,16,17] EIS experiments can be performed under conditions where these problems are avoided, and parameters quantifying transport and recombination that are required for calculating L_n can be obtained in a single experiment. For these reasons, we feel that interpretation of EIS results may be less error-prone, which is of great importance in the present study where a quantitative comparison between steady-state and dynamic techniques is attempted.

Theoretical Basis

Linearization of the Free Electron Continuity Equation. Generation, diffusive transport, and recombination of electrons in the electrolyte-filled, dye-sensitized TiO_2 layer of a DSC can be described by the continuity equation for free electrons. For steady-state conditions, this can be written as

$$\frac{dn_c(x)}{dt} = G(x) + D_n\frac{d^2n_c(x)}{dx^2} - k_n'(n_c(x) - n_{eqm})^{\gamma_n} - k_g(n_c(x) - n_{eqm})^{\gamma_g}c_{D^+}(x) = 0 \quad (1)$$

where n_c is the concentration of free electrons, $G(x)$ is the position-dependent volume photogeneration rate (typically an exponential term for Beer−Lambert light absorption), D_n is the electron diffusion coefficient, k_n' and k_g are rate constants for the recombination of electrons with triiodide and oxidized sensitizer molecules, respectively, c_{D^+} is the concentration of oxidized sensitizer molecules, γ_n and γ_g are reaction orders with respect to excess free electron concentration, and n_{eqm} is the concentration of free electrons at thermal equilibrium in the dark.

The last term in eq 1 represents recombination of electrons with oxidized sensitizer molecules. This has been included for generality and also to demonstrate that, even for the case of position-dependent recombination with oxidized sensitizer molecules, existing expressions used to determine L_n and η_{sep} from IPCE spectra remain valid for a small-perturbation measurement.

The continuity equation for oxidized sensitizer molecules can be written as

$$\frac{dc_{D^+}(x)}{dt} = G(x) - k_g(n_c(x) - n_{eqm})^{\gamma_g}c_{D^+}(x) - k_r'c_{D^+}(x) = 0 \quad (2)$$

where k_r' is the rate constant for the sensitizer regeneration reaction. In eqs 1 and 2, recombination of electrons with triiodide and regeneration of oxidized sensitizer molecules by iodide are assumed to be pseudo-first-order in free electron and oxidized sensitizer concentrations, respectively. The relevant pseudo-first-order rate constants are given by

$$k_n' = k_n c_{I_3^-} \quad (3)$$

$$k_r' = k_r c_{I^-} \quad (4)$$

where $c_{I_3^-}$ and c_{I^-} are the concentrations of triiodide and iodide in the electrolyte, respectively. Under low injection conditions, the assumption of pseudo-first-order kinetics is probably justified due to the high concentrations of triiodide and iodide typically used in the electrolyte. However, under high injection conditions, such as those obtained under AM 1.5, 1 Sun illumination, accumulation of triiodide and depletion of iodide in the pores of the TiO_2 may become important.

Solving eq 2 for c_{D^+} and substituting into eq 1 yields

$$\frac{dn_c(x)}{dt} = \eta_{reg}(n_c(x))G(x) + D_n\frac{d^2n_c(x)}{dx^2} - k_n'(n_c(x) - n_{eqm})^{\gamma_n} = 0 \quad (5)$$

where the sensitizer regeneration efficiency, η_{reg}, occurs naturally as

$$\eta_{reg}(n_c(x)) = \frac{k_r'}{k_g(n_c(x) - n_{eqm})^{\gamma_g} + k_r'} \quad (6)$$

For the case of a position-independent background generation rate, G_{bg}, and a position-independent background electron concentration, n_{bg} (from here on, referred to as "homogeneous conditions"), it is permissible to linearize eq 5 for small perturbations of $G(x)$ around G_{bg} and $n_c(x)$ around n_{bg} (Supporting Information). The resultant expression can be written in the form of the familiar electron continuity equation with a single, linear, recombination term

$$\frac{dn_c(x)}{dt} \approx \eta_{reg}(G(x) - G_{bg}) + D_n\frac{d^2n_c(x)}{dx^2} - \frac{(n_c(x) - n_{bg})}{\tau_n} \quad (7)$$

where η_{reg} is the small-perturbation sensitizer regeneration efficiency, D_n is the free electron diffusion coefficient, and τ_n is the small-perturbation free electron lifetime. Here, η_{reg} and τ_n are constants during a small-perturbation measurement but depend upon the background free electron concentration according to

$$\eta_{reg} = \frac{k_r'}{k_g n_{bg}^{\gamma_g} + k_r'} \quad (8)$$

$$\tau_n = \frac{1}{k_n' n_{bg}^{\gamma_n - 1}(\gamma_n + \gamma_g(1 - \eta_{reg}))} \quad (9)$$

For the case where the background electron concentration is provided by applying an external bias voltage to the cell instead of by illumination, the free electron lifetime is predicted to increase due to removal of the possibility of recombination with the background oxidized sensitizer population. In this case, eq 7 still holds but τ_n is replaced with

$$\tau_{n,\mathrm{dark}} = \frac{1}{\gamma_n k'_n n_{\mathrm{bg}}^{\gamma_n - 1}} \tag{10}$$

which agrees with eq 24 in ref 4. It is worth noting that, for this case, the sensitizer regeneration efficiency is not predicted to be affected by removal of background illumination and remains dependent upon the background electron concentration according to eq 8. It is also clear from eq 9 that, for $\eta_{reg} = 1$, the electron lifetime is given by eq 10; that is, the same result as if recombination of electrons with oxidized sensitizer molecules had not been considered possible.

From eq 7, it follows that, for a small perturbation of $G(x)$ and/or $n_c(x)$, under homogeneous background conditions, existing solutions to the electron continuity equation remain valid, even for $\gamma_n \neq 1$ and non-negligible recombination with oxidized sensitizer molecules. This conclusion applies to most of the commonly employed characterization techniques, provided measurements are performed under homogeneous conditions. This is usually the case for intensity-modulated photovoltage spectroscopy (IMVS),[18] small-amplitude photovoltage decay, photovoltage rise,[19,20] and electrochemical impedance spectroscopy (EIS) measurements.[21] However, this is not usually the case for intensity-modulated photocurrent spectroscopy (IMPS)[13] and small-amplitude photocurrent experiments or measurements of the IPCE under short-circuit conditions. As already mentioned, the free electron concentration in the TiO_2 layer is expected to be position-dependent under short-circuit conditions due to electron extraction at the anode.

The electron diffusion length, a characteristic length scale that arises naturally in the solution of eq 7, is defined by the expression

$$L_n = \sqrt{D_n \tau_n} \tag{11}$$

It is clear from eqs 7−11 that, if γ_n and η_{reg} are not equal to unity, L_n is dependent upon background electron concentration and also upon whether or not the measurement of L_n is made while the DSC is under background illumination.

Determination of L_n and η_{sep} from IPCE Measurements. In several recent studies, attempts have been made to determine L_n in DSCs by fitting expressions derived from eq 1, for $\gamma_n = 1$ and negligible recombination with oxidized dye molecules, to experimental IPCE data.[5,7,9] Under the conditions used for these measurements (i.e., short-circuit), linearization of eq 5 is not permissible, so if for these cells $\gamma_n \neq 1$ (which is likely to be the case), the data analysis in these studies must be considered flawed.[4,10] However, the methodological approaches and the expressions used in data fitting remain valid provided that measurement of the IPCE only results in a small perturbation of a large, spatially homogeneous, background electron concentration.

The approach used to determine L_n and η_{sep} (usually referred to as simply the electron injection efficiency) from IPCE and other optical measurements is amply described elsewhere, so only the main expressions used in the data analysis are given here.[5,22] The IPCE for substrate−electrode illumination (SEI) is given by

$$\mathrm{IPCE}_{\mathrm{SEI}}(\lambda) = \eta_{\mathrm{lh,SEI}}(\lambda)\eta_{\mathrm{sep}}(\lambda)\eta_{\mathrm{col,SEI}}(\lambda) \tag{12}$$

and for electrolyte−electrode illumination (EEI) by

$$\mathrm{IPCE}_{\mathrm{EEI}}(\lambda) = \eta_{\mathrm{lh,EEI}}(\lambda)\eta_{\mathrm{sep}}(\lambda)\eta_{\mathrm{col,EEI}}(\lambda) \tag{13}$$

In these expressions, $\eta_{lh}(\lambda)$ is the light-harvesting efficiency, $\eta_{sep}(\lambda)$ is the charge separation efficiency, and $\eta_{col}(\lambda)$ is the electron collection efficiency; the subscripts SEI and EEI represent the illumination geometry.

For Beer−Lambert light absorption by all cell components, $\eta_{lh,SEI}(\lambda)$ and $\eta_{lh,EEI}(\lambda)$ are given by

$$\eta_{\mathrm{lh,SEI}}(\lambda) = \frac{T_{\mathrm{sub}}(\lambda)\alpha_{\mathrm{D}}(\lambda)(1 - \exp[-(\alpha_{\mathrm{D}}(\lambda) + p\alpha_{\mathrm{E}}(\lambda))d])}{\alpha_{\mathrm{D}}(\lambda) + p\alpha_{\mathrm{E}}(\lambda)} \tag{14}$$

$$\eta_{\mathrm{lh,EEI}}(\lambda) = \frac{T_{\mathrm{Pt}}(\lambda)\alpha_{\mathrm{D}}(\lambda)\exp[-\alpha_{\mathrm{E}}(\lambda)s](1 - \exp[-(\alpha_{\mathrm{D}}(\lambda) + p\alpha_{\mathrm{E}}(\lambda))d])}{\alpha_{\mathrm{D}}(\lambda) + p\alpha_{\mathrm{E}}(\lambda)} \tag{15}$$

where $\alpha_D(\lambda)$ is the absorption coefficient of the dye-sensitized TiO_2 layer, $\alpha_E(\lambda)$ is the absorption coefficient of the electrolyte, $T_{sub}(\lambda)$ is the transmission of the photoanode substrate, $T_{Pt}(\lambda)$ is the transmission of the Pt-coated cathode, d is the TiO_2 layer thickness, p is the porosity of the TiO_2 layer (assumed here to be 0.5), and s is the thickness of the free electrolyte layer between the TiO_2 and the Pt-coated cathode.

Again, assuming Beer−Lambert light absorption by cell components, $\eta_{col,SEI}(\lambda)$ and $\eta_{col,EEI}(\lambda)$ are given by[5]

$$\eta_{\mathrm{col,SEI}}(\lambda) = \frac{(-L_n\alpha'(\lambda)\cosh[d/L_n] + \sinh[d/L_n] + L_n\alpha'(\lambda)\exp[-\alpha'(\lambda)d])L_n\alpha'(\lambda)}{(1 - \exp[-\alpha'(\lambda)d])(1 - L_n^2\alpha'(\lambda)^2)\cosh[d/L_n]} \tag{16}$$

$$\eta_{\mathrm{col,EEI}}(\lambda) = \frac{(L_n\alpha'(\lambda)\cosh[d/L_n] + \sinh[d/L_n] - L_n\alpha'(\lambda)\exp[-\alpha'(\lambda)d])L_n\alpha'(\lambda) \times \exp[-\alpha'(\lambda)d]}{(1 - \exp[-\alpha'(\lambda)d])(1 - L_n^2\alpha'(\lambda)^2)\cosh[d/L_n]} \tag{17}$$

where L_n is the effective electron diffusion length given by eq 11 and $\alpha'(\lambda) = \alpha_D(\lambda) + p\alpha_E(\lambda)$.

$\eta_{sep}(\lambda)$ can be defined as

$$\eta_{\mathrm{sep}}(\lambda) = \eta_{\mathrm{inj}}(\lambda)\eta_{\mathrm{reg}}(\lambda) \tag{18}$$

where $\eta_{inj}(\lambda)$ is the electron injection efficiency and $\eta_{reg}(\lambda)$ is the sensitizer regeneration efficiency. In principle, both η_{inj} and η_{reg} could be wavelength- and position-dependent in a DSC under normal operating conditions. However, provided η_{inj} is independent of photon energy, η_{sep} measured by a small-perturbation method under homogeneous conditions can reasonably be assumed wavelength- and position-independent. η_{sep} is, however, predicted to be dependent upon the background electron concentration (cf. eq 8).

It follows from eqs 12−15 that the ratio $\mathrm{IPCE}_{\mathrm{EEI}}(\lambda)/\mathrm{IPCE}_{\mathrm{SEI}}(\lambda)$ is given by

$$\frac{\mathrm{IPCE}_{\mathrm{EEI}}(\lambda)}{\mathrm{IPCE}_{\mathrm{SEI}}(\lambda)} = \frac{T_{\mathrm{Pt}}(\lambda)\exp[-\alpha_{\mathrm{E}}(\lambda)s]}{T_{\mathrm{sub}}(\lambda)}\frac{\eta_{\mathrm{col,EEI}}(\lambda)}{\eta_{\mathrm{col,SEI}}(\lambda)} \quad (19)$$

Because the parameters $\alpha_D(\lambda)$, $\alpha_E(\lambda)$, $T_{sub}(\lambda)$, $T_{Pt}(\lambda)$, and d can be determined by independent measurement (Supporting Information), eq 19 can be fitted to experimental $IPCE_{EEI}/IPCE_{SEI}$ spectra with L_n and s as the only free-fitting parameters. We note that, in other studies, the free electrolyte layer thickness, s, is usually taken as a known parameter. However, we choose to allow this parameter to vary as it improves fits to spectra at wavelengths where the electrolyte is strongly absorbing. Provided the value of s is reasonably close to the nominal value, it does not strongly influence the value of L_n required to obtain a fit. Once L_n is known, eqs 12 and 13 can be fitted to individual $IPCE_{SEI}$ and $IPCE_{EEI}$ spectra, respectively, with η_{sep} (assumed here to be wavelength-independent) as the only free-fitting parameter.

Determination of L_n from EIS Measurements. An alternative approach for determination of L_n is based upon the technique of EIS. EIS spectra of DSCs can be modeled by the equivalent circuit shown in Figure 1.

Bisquert has shown that the impedance of the central transmission line shown in Figure 1 (outlined by the red box) is equivalent to that derived by solution to the free electron continuity equation.[23] The local resistance to electron transport in the TiO_2 layer is represented by the distributed resistance r_t (total resistance $R_t = r_t d$) and is determined by the conductivity of the TiO_2, which is, in turn, related to the carrier concentration (n_c) and diffusion coefficient (D_n). The local resistance to charge transfer across the TiO_2−electrolyte interface is represented by the distributed component r_{ct} (total resistance $R_{ct} = r_{ct}/d$) and is determined by n_c and the free electron lifetime (τ_n). Bisquert has shown that L_n is related to R_t and R_{ct} by

$$L_n = d\sqrt{\frac{R_{ct}}{R_t}} \quad (20)$$

In principle, this quantity is equal to that given by eq 11, which can be determined by analysis of IPCE spectra, as described in the previous subsection. The main aim of the work presented in this article was to test whether this is, in fact, found to be the case experimentally, given that there has recently been some controversy surrounding the determination of L_n by dynamic relaxation techniques. Of course, it is also an important test of any device model that the predictions made about steady-state behavior are in agreement with those made about dynamic behavior.

Experimental Methods

Fabrication of Dye-Sensitized Solar Cells. Nanocrystalline TiO_2 electrodes were fabricated on fluorine-doped tin oxide coated glass substrates (FTO, Pilkington TEC-15) cut into 1.5 cm × 2.5 cm pieces and cleaned by sequential sonication in 5% Decon 90 solution, distilled water, propan-2-ol, and absolute ethanol. Compact TiO_2 blocking layers were deposited on the FTO substrates by spray pyrolysis of a 0.2 M solution of titanium(IV)bis(acetoacetonato)di(isopropanoxylate) in ethanol. Spraying was carried out using a hand-held aspirator driven by a vacuum pump with a spraying protocol of two sprays every 10 s for 2 min. Electrodes were then soaked in a 40 mM solution of $TiCl_4$ in distilled water (prepared by dilution of a 2 M stock solution that was prepared at ca. 0 °C) for 30 min at 80 °C. After rinsing in distilled water and drying, a ca. 12 μm layer of nanocrystalline TiO_2 was deposited by successive screen printing using a TiO_2 paste consisting of Degussa P25 TiO_2 powder and an ethyl cellulose binder in α-terpinol. TiO_2 layers were gradually heated to 450 °C, where they were held for 15 min before being heated to 500 °C for a further 15 min. Electrodes were subjected to a second identical treatment in $TiCl_4$ solution, rinsed, dried, and heated to ca. 450 °C in a hot air stream for 30 min. Once electrodes had cooled to ca. 100 °C, they were immersed into a 0.15 mM solution of *cis*-disothiocyanato-(2,2′-bipyridyl-4,4′-dicarboxylic acid)-(2,2′-bipyridyl-4,4′-dinonyl) ruthenium(II) (Z907, Dyesol) in 1:1 acetonitrile/*tert*-butanol and left overnight before being removed and rinsed in acetonitrile.

Platinized counter electrodes were fabricated on identical pieces of FTO with small holes drilled into one corner. After cleaning, a thin layer of Pt was deposited onto the FTO by thermal decomposition of hexachloroplatinic acid.

Dye-sensitized TiO_2 electrodes and counter electrodes were sealed together in a sandwich configuration using a hot-melt polymer (Surlyn, DuPont). The interelectrode space was filled with an electrolyte by vacuum backfilling. Holes were sealed using a small piece of hot-melt polymer and a microscope coverslip.

Electrolytes were all 0.1 M I_2 in 3-methoxypropionitrile with varying concentrations of propylmethylimiddazolium iodide (PMII), LiI, lithium bis(trifluormethane)sulfonidime (LiTFSI), and *N*-methylbenzimidazole (NMB). Details of exact electrolyte compositions are given in the text where relevant.

Characterization Techniques. IPCE spectra were measured with a spectral resolution of ca. 5 nm using a probe light source consisting of a 300 W xenon lamp and grating monochromator equipped with order-sorting filters (Newport/Oriel). The incident photon flux was determined using a calibrated silicon photodiode (Newport/Oriel). Measurements were performed while the cell was under background illumination from a high-power red light-emitting diode (LED, λ = 627 nm, 19.2 nm fwhm). At this illumination wavelength, the absorption length of light in the TiO_2 layer is calculated to be ca. 12 μm, approximately equal to the TiO_2 layer thicknesses used in this study. The probe and background light intensities were adjusted so that the average volume photoexcitation rate induced in the cell by the probe light was at most 1.8% of that induced by the background light. During measurements, cells were also biased such that the applied voltage was equal to the open-circuit photovoltage (V_{OC}) induced by the background illumination. Different background illumination intensities were achieved using a set of neutral density filters (Newport) through which both background and probe lights were passed to ensure the probe-to-background intensity ratio remained unaltered with varying background illumination intensity.

When measurements were performed for both substrate−electrode illumination (SEI) and electrolyte−electrode illumination (EEI), the background light intensity was slightly adjusted

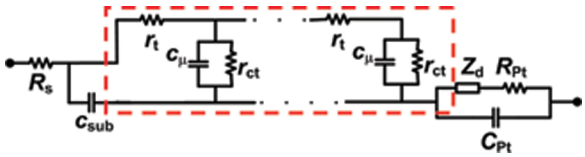

Figure 1. Equivalent circuit used to model EIS spectra of DSCs. The transmission line that models diffusion and recombination in the TiO_2 layer is outlined by the red box; the components r_t and r_{ct} are discussed in the main text. Also included in the model are components representing the distributed capacitance of the TiO_2 (c_μ), the device series resistance (R_s), the substrate capacitance (C_{sub}), the Warburg impedance due to diffusion of redox species in the electrolyte (Z_d), the resistance to charge transfer at the Pt-coated counter electrode (R_{Pt}), and the capacitance of the electrical double layer at the counter electrode (C_{Pt}).

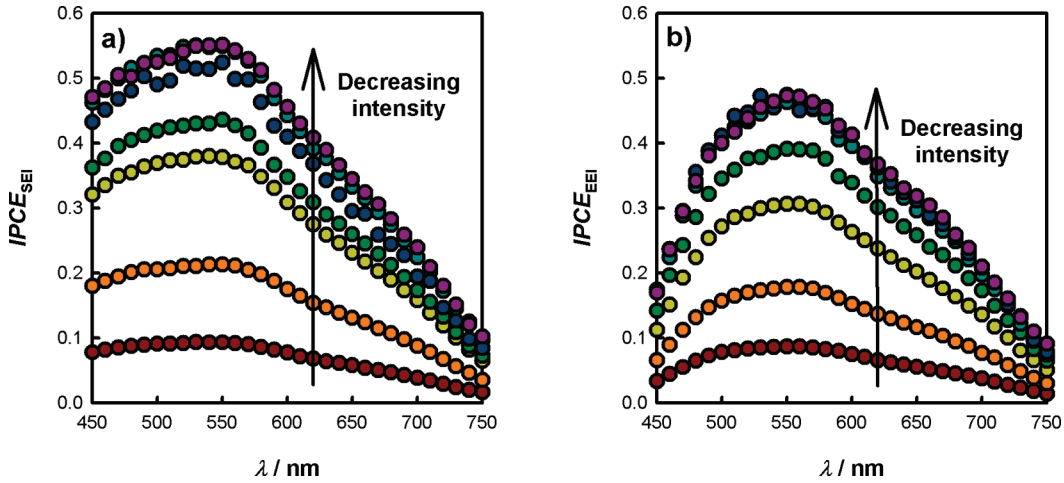

Figure 2. Typical dependence of IPCE spectra (measured under close to open-circuit conditions) on the background light intensity for substrate−electrode illumination (a) and electrolyte−electrode illumination (b). The background light intensities used covered a range equivalent to ca. 0.001−1 Sun.

after changing from SEI to EEI, by varying the LED driving current, to ensure exactly the same V_{OC} for both measurements. The adjustment was small in all cases and is thought to correct for differences in attenuation of the background light by the photoanode substrate and the Pt-coated cathode, ensuring that the intensity of the background illumination incident on the dye-sensitized TiO_2 layer itself is equal for both SEI and EEI.

Photocurrents were amplified using a Stanford SR570 low-noise current preamplifier, and the probe light was chopped at a frequency $f = 0.333$ Hz using a mechanical chopper controlled by a Stanford SR830 lock-in amplifier. This chopping frequency was found to be low enough to prevent significant attenuation of the cell's photocurrent over the intensity/V_{OC} range studied here. Any measurements where the photocurrent from the cell was observed to lag behind that of the silicon photodiode by more than 10° were discarded (attenuation of photocurrent by ca. 2% is predicted for this phase lag, assuming simple RC attenuation).

V_{OC}-intensity characteristics and EIS spectra were measured using an Autolab potentiostat/galvanostat and the Nova 1.5 software package. EIS experiments were performed under illumination provided by a red LED ($\lambda = 627$ nm, 19.2 nm fwhm) while the cell was biased at the V_{OC} induced by the illumination. Different illumination intensities were achieved using neutral density filters mounted in an automated filter wheel system (Newport) that was controlled by the Nova 1.5 software.

The thickness of the nanocrystalline TiO_2 layers was determined by profilometry measurements using an Alpha-Step IQ surface profiler. Transmission spectra of dye-sensitized TiO_2 layers, Pt-coated electrodes, and FTO substrates coated with compact TiO_2 blocking layers were measured using a Shimadzu SolidSpec-3700 UV−vis-NIR spectrophotometer equipped with an integrating sphere. Absorption spectra of 100-fold dilute electrolyte solutions were measured using a Varian Cary 5000 UV−vis-NIR spectrophotometer.

Results and Discussion

Determination of L_n by Analysis of IPCE Spectra. Figure 2 shows $IPCE_{SEI}$ and $IPCE_{EEI}$ spectra for a DSC with an electrolyte composed of 2 M LiI and 0.1 M I_2 in 3-MPN. Spectra were measured under close to open-circuit conditions with a 627 nm background illumination and an intensity range of ca. 0.05−50 mW cm^{-2}. The range of photogeneration rates produced by the background illumination is calculated to be equivalent to that produced by AM 1.5 illumination in the intensity range of ca. 0.1−100 mW cm^{-2} (i.e., 0.001−1 Sun). As the background light intensity was increased, the IPCE at all wavelengths was found to markedly decrease. This behavior was found for all DSCs studied here, regardless of illumination geometry, electrolyte composition, and whether or not the cell was equipped with a compact TiO_2 blocking layer.

Because these data are obtained under close to open-circuit conditions, they are not directly comparable to measurements made at different light intensities under short-circuit conditions. Indeed, the trend of decreasing IPCE with increasing intensity shown in Figure 2 is *opposite* to that often found for DSCs exhibiting poor charge collection when IPCE measurements are made under short-circuit conditions.[7,9,10] We will later show that the intensity and voltage dependences of the IPCE observed here are predominantly caused by a drop in η_{sep} as the concentration of electrons in the TiO_2 layer increases.

Figure 3a shows $IPCE_{EEI}/IPCE_{SEI}$ ratio spectra for a DSC with an electrolyte consisting of 0.9 M propylmethylimidazolium iodide (PMII), 0.1 M LiI, and 0.1 M I_2 in 3-methoxypropionitrile (3-MPN). Spectra are well fitted by assuming $\eta_{col} = 1$ for all wavelengths (i.e., $L_n \gg d$) and simply considering the difference in optical losses between EEI and SEI.

The data in Figure 3a clearly show that, for this electrolyte, L_n is long enough to render the charge collection almost 100% efficient under all conditions studied. However, as a consequence of this, no more information about the exact magnitude of L_n or its intensity/V_{OC} dependence can be obtained from these data. This highly efficient charge collection was observed for all DSCs with electrolytes containing 1 M PMII or LiI and 0.1 M I_2 with no other additives and also for DSCs with an electrolyte containing 1 M PMII, 0.1 M I_2, 0.1 M LiTFSI, and 0.5 M NMB.

Another quite different behavior was obtained for an aged DSC containing 2 M LiTFSI in the electrolyte, without the addition of NMB (Figure 3b). At wavelengths where the sensitizer absorbs strongly, the $IPCE_{EEI}/IPCE_{SEI}$ ratio is significantly lower than that predicted by considering optical losses alone. Spectra are similar for all background light intensities, and no clear trend with varying background intensity is found. Fitting eq 19 to the data yields values of L_n in the range of 5−7 μm.

A third type of behavior was observed for an aged DSC containing 0.1 M LiTFSI in the electrolyte, again without the addition of NMB (Figure 3c). A clear trend of decreasing

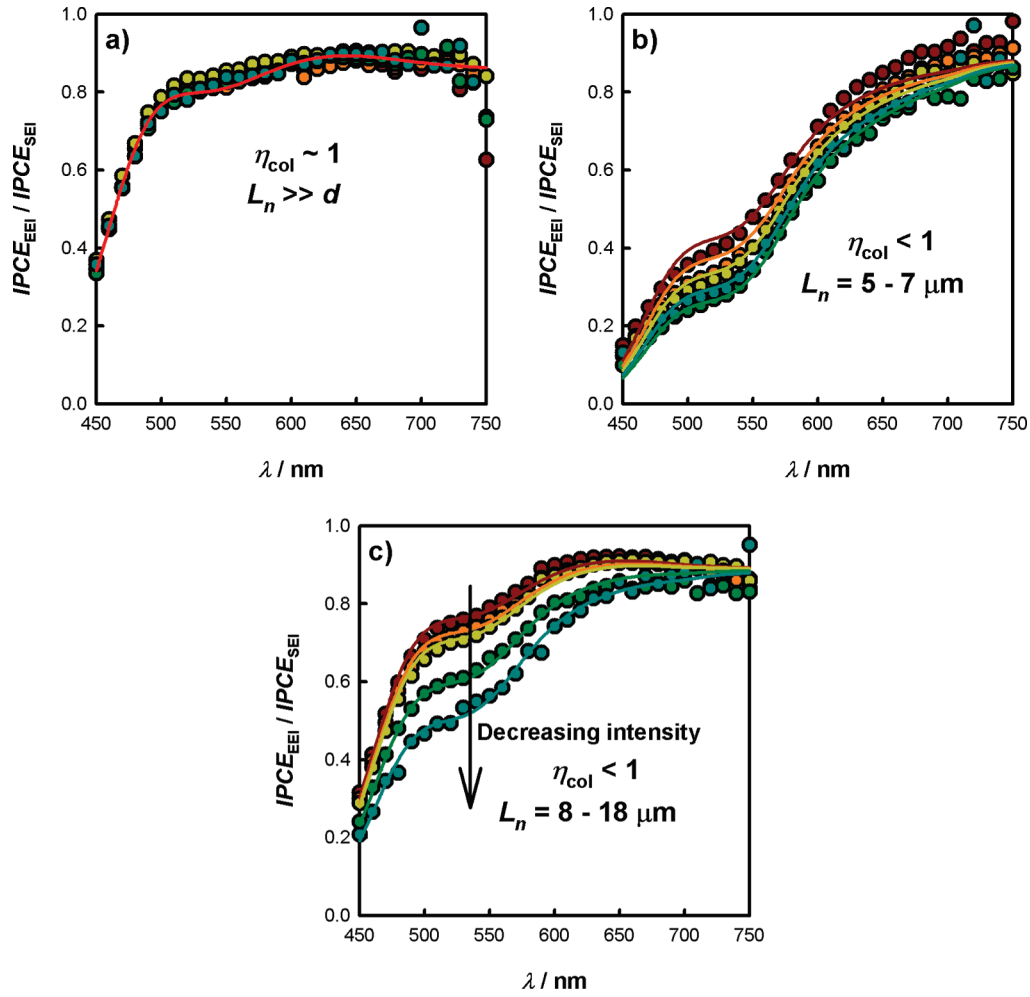

Figure 3. $IPCE_{EEI}/IPCE_{SEI}$ ratio spectra measured under close to open-circuit conditions with background light intensities covering a range equivalent to ca. 0.01−1 Sun. Lines are fits using eq 19. The electrolyte compositions of the DSCs were 0.9 M PMII, 0.1 M LiI, and 0.1 M I_2 in 3-MPN (a), 1 M PMII, 0.1 M I_2, and 2 M LiTFSI in 3-MPN (b), and 1 M PMII, 0.1 M I_2, and 0.1 M LiTFSI in 3-MPN (c).

$IPCE_{EEI}/IPCE_{SEI}$ ratio with decreasing intensity can be observed for this DSC, and fitting eq 19 to the data yields L_n in the range of 8−18 μm. Data could be fitted to obtain L_n with a good degree of statistical confidence over ca. 2 orders of magnitude of background light intensity (range of ca. 0.01−1 Sun). Reliable $IPCE_{EEI}$ data (i.e., negligible phase shift of the DSC's photocurrent with respect to the Si reference photodiode) for lower light intensities could not be obtained at the chopping frequency used.

Determination of L_n by EIS. For comparison with results obtained by fitting IPCE spectra, L_n has been determined for the DSCs discussed in the previous subsection at a range of different background light intensities by fitting data obtained from EIS experiments with the equivalent circuit shown in Figure 1. The EIS experiments were performed under the same homogeneous conditions as for the IPCE experiments. Under these conditions, the transmission line model should be valid (distributed circuit elements take on the same value throughout the TiO_2 layer because the electron concentration is approximately position-independent) so that L_n can be reliably determined provided it is not much shorter than the TiO_2 layer thickness. For the case of $L_n \ll d$, the transmission line is described by a Gerischer impedance and values of R_{ct} and R_t cannot be independently determined.[23] In this study, spectra resembling those of a Gerischer impedance were observed. However, fits to these spectra with unique values of R_t and R_{ct} could still be obtained for $L_n \geq d/2$, and estimated errors in the fitted parameters were in all cases <30% of the parameter values. The validity of these fitting results is further supported by the fact that the voltage dependence of fitted parameters on changing from $L_n > d$ to $L_n < d$ remains continuous.

To fit EIS data, the parameters associated with the Pt-coated cathode, diffusion in the electrolyte, and the capacitance of the substrate were determined by independent "blank" experiments using thin-layer cells that did not include the sensitized TiO_2 layer. Averaged parameters were used as initial values during data fitting for complete DSCs, and care was taken to ensure that these parameters did not vary by an unphysical amount compared with the corresponding values obtained in the "blank" experiments. Capacitors in the model were replaced by constant phase elements (CPE) to improve the quality of the fits, and values of the CPE exponent were found to be in the range of 0.85−1. Fits were also performed with these exponents fixed to 1 to investigate the influence of this parameter on the values of R_{ct} and R_t obtained. In all cases, the value of L_n calculated from R_{ct} and R_t using eq 20 was found to be relatively insensitive to whether or not CPEs were used during the fitting. Representative examples of EIS spectra and fits to the transmission line model are shown in Figure 4.

Typically, R_{ct} and R_t were found to vary exponentially with V_{OC}, as is frequently observed for DSCs.[11] This continuous variation of parameters with externally imposed conditions provides some measure of confidence in the fitting results. The slopes of semilogarithmic plots of R_t versus V_{OC} were found to

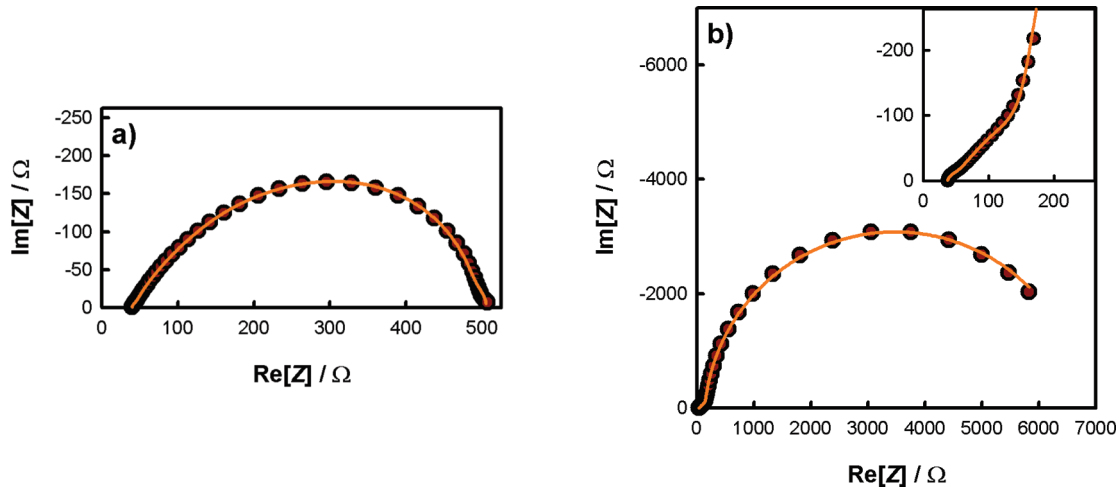

Figure 4. Electrochemical impedance spectra and fits to the transmission line model for DSCs with relatively short (electrolyte containing 2 M LiTFSI) (a) and long (electrolyte containing 2 M LiI) (b) L_n compared with the TiO_2 layer thickness.

be approximately equal for all electrolyte compositions (with the exception of the electrolyte containing 2 M LiTFSI) over a voltage range of at least 0.2 V, with a mean value of 16.2 V^{-1}. This is in good agreement with the theoretical value of 16.9 V^{-1} predicted for the expected conduction band transport mechanism,[11] further increasing confidence in the reliability of the EIS fitting results.

In contrast to the results obtained for R_t, the dependence of R_{ct} on V_{OC} was strongly influenced by the electrolyte composition. Neglecting for the moment the predicted influence of recombination with oxidized sensitizer molecules, the dependence of R_{ct} on cell voltage is expected to be determined by γ_n. For $\gamma_n = 1$, $d\log_{10}(R_{ct})/dV_{OC}$ is predicted to be 16.9 V^{-1} at 298 K. For a reaction order of $\gamma_n < 1$, $d\log_{10}(R_{ct})/dV_{OC}$ is predicted to be <16.9 V^{-1}. For the DSCs studied here, slopes on semilogarithmic plots of R_{ct} versus V_{OC} were found to be in the range of 11.0−16.9 V^{-1}, corresponding to γ_n in the range of 0.65−1. Figure 5a,b shows the dependences of R_t and R_{ct} on V_{OC} for the DSCs studied here. The dependence of the TiO_2 chemical capacitance (C_μ) on V_{OC} is shown in Figure S2 (Supporting Information).

At this point, it is worthwhile to examine the dependence of V_{OC} on the incident photon flux (I_0), which also provides important information regarding the recombination mechanism.[24,25] Figure 5c shows the dependence of V_{OC} on I_0 for the DSCs studied here. For $\gamma_n = 1$, $dV_{OC}/d\log_{10}(I_0)$ is predicted to be 59 mV at 298 K. The plots in Figure 5c exhibit slopes of 62−67 mV for cells containing 2 M Li^+ (for both LiI and LiTFSI), whereas for cells with a lower Li^+ concentration, greater slopes of up to 89 mV are found. We have previously shown, using a model proposed by Salvador et al.,[24] that this variation in γ_n can be explained by considering a transition from surface-state-mediated recombination to conduction-band-mediated recombination as the conduction band edge is shifted toward the electrolyte redox level by adsorption of Li^+ on the TiO_2 surface.[26] Others have suggested that unpinning of the conduction band edge or nonideal electron statistics can also explain an apparent $\gamma_n \neq 1$.[17,27] Here, we have taken the approach of calculating an average, effective reaction order with respect to conduction band electrons and do not further consider the physical origin of this reaction order.

Figure 5d shows a comparison of recombination reaction orders obtained from $R_{ct}-V_{OC}$ data (γ_{EIS}) and $V_{OC}-I_0$ data (γ_{VOC-I_0}). Reaction orders obtained by the different approaches are in good agreement, which is clear evidence that R_{ct} derived by fitting EIS data is useful in describing the steady-state recombination process in DSCs.

Now that the reliability of the EIS fitting results has been established (by comparison with theory for R_t-V_{OC} data and by comparison to steady-state $V_{OC}-I_0$ characteristics for $R_{ct}-V_{OC}$ data), we can confidently use eq 20 to calculate L_n. Figure 6 shows the dependence of L_n on V_{OC} for the DSCs studied here.

As a result of the equal dependences of R_t and R_{ct} on V_{OC}, L_n is found to be independent of V_{OC} for cells with electrolytes containing a high LiI concentration over a voltage range of ca. 0.2 V (corresponding to an intensity range spanning ca. 3 orders of magnitude), whereas for cells with electrolytes containing little or no Li^+, a significant increase in L_n with increasing V_{OC} is found. For the aged cell containing 2 M LiTFSI, a slight decrease in L_n with V_{OC} is observed as a result of the nonideal R_t-V_{OC} characteristics for this cell. The origin of this is unclear, although it may be an artifact of the data fitting as L_n is found to be in the range where independent determination of R_{ct} and R_t begins to become difficult. The larger error estimates for these data partly reflect this fact.

Comparison of Steady-State and Dynamic Methods for Determining L_n. Combining the results obtained by analysis of IPCE and EIS data in the previous subsections allows for a direct comparison between L_n determined by steady-state and dynamic relaxation methods. Figure 7 shows the dependence of L_n on V_{OC} obtained using the two different techniques for aged DSCs with electrolytes containing 1 M PMII, 0.1 M I_2, and either 0.1 M LiTFSI or 2 M LiTFSI. The IPCE and EIS experiments, from which the data in Figure 7 were obtained, were performed successively on the same day, and the combined measurement duration was ca. 14 h for each DSC. The DSCs used had also been aged for several weeks prior to performing the experiments. For these reasons, we believe that any transient variation in L_n due to the inherent instability of some DSCs has been minimized in our measurements.

For the DSC with an electrolyte containing 0.1 M LiTFSI, IPCE-derived L_n data are in excellent agreement with EIS-derived L_n data. Values obtained by the different techniques agree to better than a factor of 1.3 over the entire voltage range studied, in much closer agreement than previously reported L_n data where differences between techniques of up to a factor of 2−3 have been found.

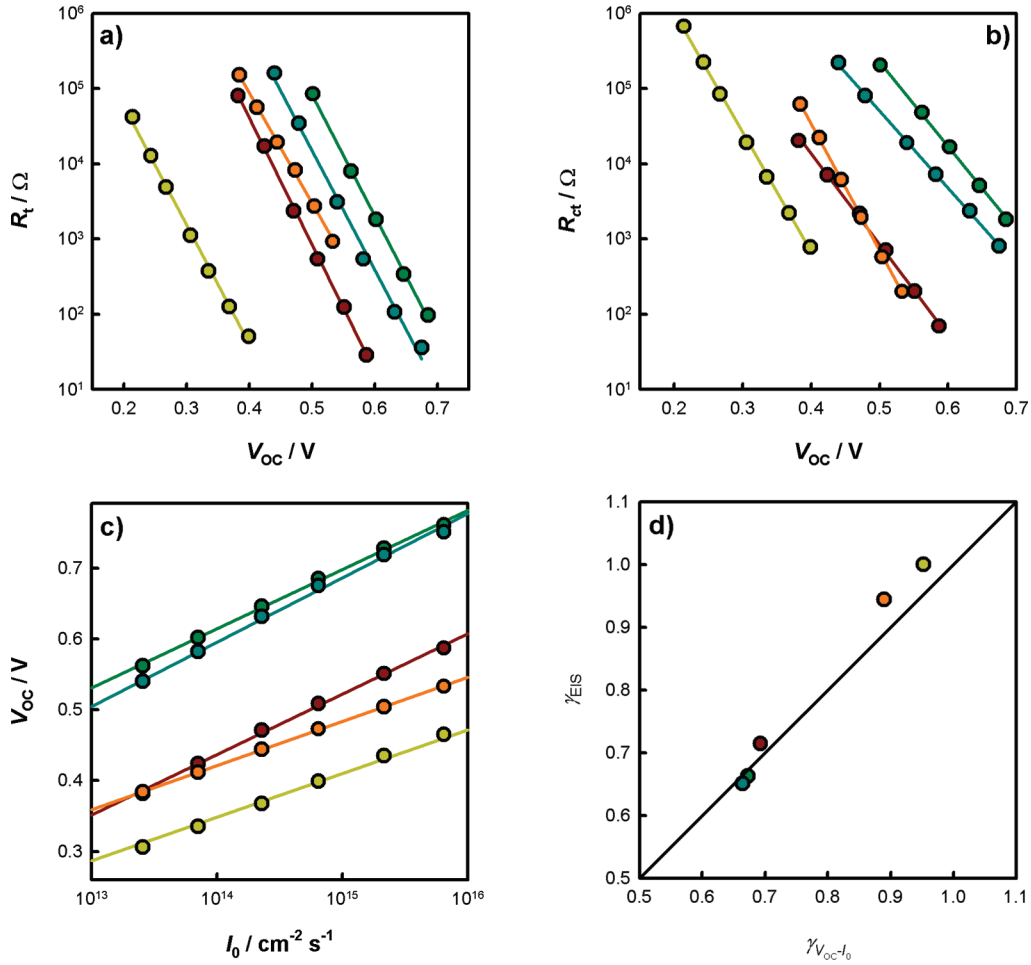

Figure 5. Dependence of R_t (a) and R_{ct} (b) on V_{OC} and dependence of V_{OC} on I_0 (c) for cells with electrolytes containing no additives (green), 0.1 M LiTFSI (red), 0.1 M LiTFSI and 0.5 M NMB (blue), 2 M LiTFSI (orange), and 2 M LiI (yellow). Also shown is the correlation between recombination reaction orders derived from $R_{ct}-V_{OC}$ data and from $V_{OC}-I_0$ data (d); the expected unit slope is indicated by the black line.

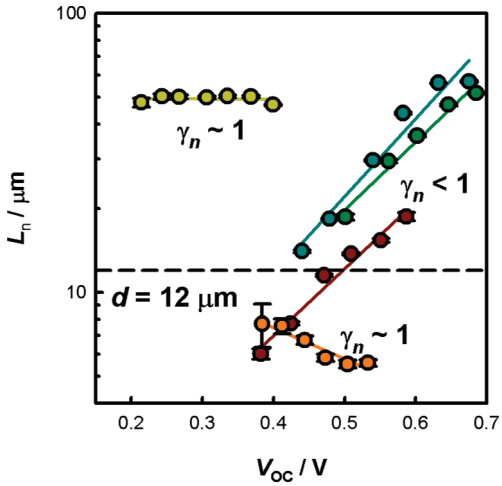

Figure 6. Dependence of L_n on V_{OC} for DSCs with electrolytes containing no additives (green), 0.1 M LiTFSI (red), 0.1 M LiTFSI and 0.5 M NMB (blue), 2 M LiTFSI (orange), and 2 M LiI (yellow). The TiO_2 layer thickness, $d = 12$ μm, is indicated by the dashed line.

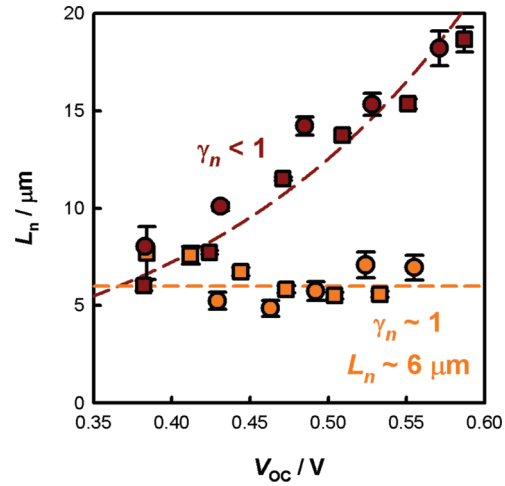

Figure 7. Comparison between L_n determined by steady-state and dynamic methods for DSCs with electrolytes containing 0.1 M LiTFSI (red) and 2 M LiTFSI (orange). Circles and squares represent L_n determined by analysis of IPCE data and EIS data, respectively. The dashed lines represent L_n calculated from exponential fits to R_t-V_{OC} and $R_{ct}-V_{OC}$ data (red) or the mean value of L_n (orange).

No clear correlation in L_n with V_{OC} can be observed for the DSC containing 2 M LiTFSI, and values obtained by the two techniques disagree by no more than a factor of 1.6 at the extremes of the two distributions of values. The average value of L_n is 6.1 μm (indicated by the dashed orange line in Figure 7), with a standard deviation of 0.9 μm. Given that, for this DSC, the average value of γ_n is 0.97 (determined from $V_{OC}-I_0$ and $R_{ct}-V_{OC}$ data), it seems reasonable to conclude that L_n for this cell is approximately independent of bias voltage. Interestingly, this was also found for the DSC containing 2 M LiI in the electrolyte, indicating that whatever causes the decrease in

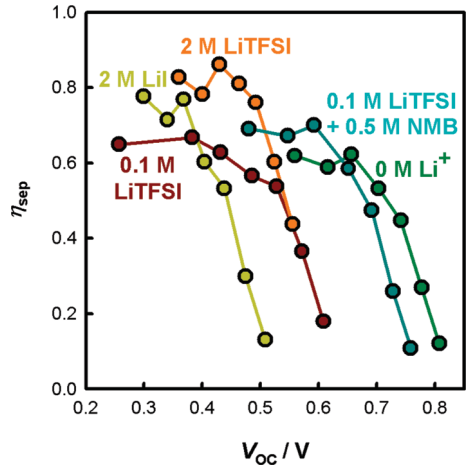

Figure 8. Dependence of η_{sep} on V_{OC} for DSCs with electrolytes containing no additives (green), 0.1 M LiTFSI (red), 0.1 M LiTFSI and 0.5 M NMB (blue), 2 M LiTFSI (orange), and 2 M LiI (yellow).

L_n upon changing from LiI to LiTFSI does not influence γ_n. It is also worth noting that the influence of the Li^+ source on L_n varies with aging. Freshly fabricated DSCs with LiTFSI and LiI exhibit similar L_n, but over the first couple of days of aging, L_n decreases (while still remaining approximately intensity-independent) for DSCs containing 2 M LiTFSI in the electrolyte. These unexpected phenomena are currently under investigation in our laboratory.

For cells without LiTFSI in the electrolyte, the exact magnitude of L_n cannot be established from the IPCE data at most intensities studied because $\eta_{col} \approx 1$ for these cells. However, the inequality $L_n \gg d$ is confirmed by both IPCE and EIS data. Given the good agreement between techniques for cells where L_n can be determined from both IPCE and EIS data, we propose that L_n determined by EIS for the other DSCs is very likely to be correct.

The prediction of short-circuit photocurrent produced under 1 Sun illumination based on these L_n values is nontrivial as they are only applicable to the particular (homogeneous) conditions at which they were determined. However, it is reasonable to expect some correlation between L_n and short-circuit photocurrent; for example, DSCs exhibiting diffusion lengths that are always shorter than the TiO_2 layer thickness would be expected to produce lower photocurrents than DSCs that exhibit diffusion lengths that are always much longer than the TiO_2 layer thickness. Unsurprisingly, this was found to be the case here, with DSCs employing LiTFSI-containing electrolytes exhibiting consistently lower photocurrents than DSCs employing LiI-containing electrolytes (Supporting Information).

Variation of η_{sep} with V_{OC}. The knowledge of L_n (which we have now shown to be reliable) combined with IPCE measurements and optical characterization enables the determination of η_{sep} by fitting eqs 12 and 13 to individual $IPCE_{SEI}$ and $IPCE_{EEI}$ spectra. Figure 8 shows the dependence of η_{sep} on V_{OC} for the DSCs discussed in the previous sections. L_n values used in the determination of η_{sep} at the two lowest photovoltages for the 0.1 and 2 M LiTFSI DSCs were estimated by extrapolation of $L_n - V_{OC}$ plots. This was necessary because L_n could not be determined at these photovoltages as the cell response time was too slow to obtain reliable $IPCE_{EEI}$ spectra at the chopping frequency used. However, $IPCE_{SEI}$ spectra over strongly absorbed wavelengths could be obtained, which together with the extrapolated L_n values were used to estimate η_{sep}. For higher photovoltages or other electrolyte compositions, no extrapolation of $L_n - V_{OC}$ plots was necessary.

For all cells, η_{sep} is found to increase with decreasing V_{OC}, before it begins to saturate at the lowest voltages studied. A trend of increasing maximum η_{sep} with increasing Li^+ concentration can also be observed, consistent with several other studies that indicate that addition of Li^+ to the electrolyte can increase the electron injection efficiency, the sensitizer regeneration efficiency, or both.[7,22,28−30]

The marked decrease in η_{sep} with increasing V_{OC} may arise from a number of factors, such as a decrease in η_{inj} caused by a diminishing density of acceptor states as charge accumulates in the TiO_2 or a charge-induced shift in the TiO_2 energy levels relative to the sensitizer excited state levels. However, Koops et al. have shown that, for DSCs employing the N719 sensitizer, η_{inj} only weakly decreases with increasing negative bias, with a maximum decrease of only 8% for bias voltages several hundred millivolts negative of the V_{OC} obtained under AM 1.5, 1 Sun illumination.[22] It, therefore, seems unlikely that the dramatic decrease in separation efficiency is caused solely by a diminishing η_{inj}.

It is also possible that a voltage-dependent energy barrier at the FTO−TiO_2 interface could result in an apparent decrease in η_{sep} with increasing V_{OC}.[31,32] In this case, the quantity η_{sep} cannot be identified with a charge separation efficiency according to eq 18, and the model presented here would require modification. However, we rule out the possibility of a barrier to electron extraction causing an apparent decrease in η_{sep} on the basis that the same phenomenon is observed for DSCs with and without compact TiO_2 blocking layers (data not shown). In addition, there is no evidence for a voltage-dependent energy barrier in the EIS spectra obtained for these DSCs, which are well fitted by the transmission line model (Figure 1) without the need to include additional circuit elements to represent the FTO−TiO_2 contact.

The most likely remaining possibility for the decrease in η_{sep} with increasing negative bias is that η_{reg} decreases with increasing background electron concentration in the TiO_2, as predicted by eq 8. Consistent with this explanation, Haque et al. have found that the rate of decay of the oxidized sensitizer concentration, following photoexcitation of a dye-sensitized TiO_2 layer immersed in a redox inactive electrolyte, increases as the TiO_2 electrode is biased increasingly more negative. They remark that the observed voltage dependence of the decay kinetics is consistent with a reaction occurring between oxidized sensitizer molecules and electrons accumulated in the TiO_2 layer as a result of the applied bias.[33] We hope to report shortly on a more detailed study into the factors influencing sensitizer regeneration efficiency and its impact on the steady-state current−voltage characteristics of DSCs.

Conclusions

L_n in DSCs determined by EIS is found to be in good agreement with L_n determined by steady-state IPCE measurements, under conditions where linearization of the free electron continuity equation is permissible. These results show that dynamic relaxation techniques do not fail to correctly predict L_n in nanoporous photoelectrodes,[9] provided that care is taken to ensure that assumptions made in data analysis are valid. The results also confirm suggestions that the origin of previously observed discrepancies in L_n values between dynamic relaxation techniques and steady-state techniques is caused by failure to properly account for nonlinear recombination kinetics.[4,10]

In addition, the good agreement between frequency-domain (EIS) and steady-state measurements (IPCE and $V_{OC} - I_0$ char-

acteristics) provides an important experimental confirmation that the simple diffusion−recombination model used to describe DSC operation is basically correct. However, it is important to realize that L_n obtained by the methods used here is of limited relevance to actual device operation.

It has also been shown that, for DSCs employing the Z907 sensitizer and 3-MPN-based electrolytes, the charge separation efficiency decreases with increasing V_{OC}. This effect is probably a result of decreasing sensitizer regeneration efficiency as electrons accumulate in the TiO_2 and the rate of recombination of electrons with oxidized sensitizer molecules increases. It is, therefore, possible that the V_{OC} and fill factor of DSCs may be influenced by inefficient sensitizer regeneration, even if the sensitizer regeneration efficiency under short-circuit conditions is close to unity.

Acknowledgment. This work was supported by NUS and Nanocore start-up grants (R-284-000-064-133/R-284-000-066-646) and a URC research grant (R-284-000-075-112).

Supporting Information Available: Details of the linearization of the electron continuity equation, optical data used in the determination of L_n and η_{sep} from IPCE data, capacitance data obtained from EIS experiments, and current−voltage characteristics of DSCs measured under AM 1.5, 1 Sun illumination. This material is available free of charge via the Internet at http://pubs.acs.org.

References and Notes

(1) O'Regan, B.; Grätzel, M. *Nature* **1991**, *353*, 737–740.
(2) Chiba, Y.; Islam, A.; Watanabe, Y.; Komiya, R.; Koide, N.; Han, L. Y. *Jpn. J. Appl. Phys., Part 2* **2006**, *45*, L638–L640.
(3) Fukui, A.; Fuke, N.; Komiya, R.; Koide, N.; Yamanaka, R.; Katayama, H.; Han, L. Y. *Appl. Phys. Express* **2009**, *2*, 3.
(4) Bisquert, J.; Mora-Seró, I. *J. Phys. Chem. Lett.* **2010**, *1*, 450–456.
(5) Halme, J.; Boschloo, G.; Hagfeldt, A.; Lund, P. *J. Phys. Chem. C* **2008**, *112*, 5623–5637.
(6) Sodergren, S.; Hagfeldt, A.; Olsson, J.; Lindquist, S. E. *J. Phys. Chem.* **1994**, *98*, 5552–5556.
(7) Barnes, P. R. F.; Anderson, A. Y.; Koops, S. E.; Durrant, J. R.; O'Regan, B. C. *J. Phys. Chem. C* **2009**, *113*, 1126–1136.
(8) Wang, H. X.; Peter, L. A. *J. Phys. Chem. C* **2009**, *113*, 18125–18133.
(9) Barnes, P. R. F.; Liu, L.; Li, X.; Anderson, A. Y.; Kisserwan, H.; Ghaddar, T. H.; Durrant, J. R.; O'Regan, B. C. *Nano Lett.* **2009**, *9*, 3532–3538.
(10) Villanueva-Cab, J.; Wang, H.; Oskam, G.; Peter, L. M. *J. Phys. Chem. Lett.* **2010**, *1*, 748–751.
(11) Wang, Q.; Ito, S.; Grätzel, M.; Fabregat-Santiago, F.; Mora-Sero, I.; Bisquert, J.; Bessho, T.; Imai, H. *J. Phys. Chem. B* **2006**, *110*, 25210–25221.
(12) Leng, W. H.; Barnes, P. R. F.; Juozapavicius, M.; O'Regan, B. C.; Durrant, J. R. *J. Phys. Chem. Lett.* **2010**, *1*, 967–972.
(13) Dloczik, L.; Ileperuma, O.; Lauermann, I.; Peter, L. M.; Ponomarev, E. A.; Redmond, G.; Shaw, N. J.; Uhlendorf, I. *J. Phys. Chem. B* **1997**, *101*, 10281–10289.
(14) Peter, L. M. *Phys. Chem. Chem. Phys.* **2007**, *9*, 2630–2642.
(15) Peter, L. M. *J. Phys. Chem. C* **2007**, *111*, 6601–6612.
(16) Bisquert, J.; Vikhrenko, V. S. *J. Phys. Chem. B* **2004**, *108*, 2313–2322.
(17) Jennings, J. R.; Ghicov, A.; Peter, L. M.; Schmuki, P.; Walker, A. B. *J. Am. Chem. Soc.* **2008**, *130*, 13364–13372.
(18) Schlichthorl, G.; Huang, S. Y.; Sprague, J.; Frank, A. J. *J. Phys. Chem. B* **1997**, *101*, 8141–8155.
(19) O'Regan, B. C.; Bakker, K.; Kroeze, J.; Smit, H.; Sommeling, P.; Durrant, J. R. *J. Phys. Chem. B* **2006**, *110*, 17155–17160.
(20) Dunn, H. K.; Peter, L. M. *J. Phys. Chem. C* **2009**, *113*, 4726–4731.
(21) Bisquert, J.; Garcia-Belmonte, G.; Fabregat-Santiago, F.; Ferriols, N. S.; Bogdanoff, P.; Pereira, E. C. *J. Phys. Chem. B* **2000**, *104*, 2287–2298.
(22) Koops, S. E.; O'Regan, B. C.; Barnes, P. R. F.; Durrant, J. R. *J. Am. Chem. Soc.* **2009**, *131*, 4808–4818.
(23) Bisquert, J. *J. Phys. Chem. B* **2002**, *106*, 325–333.
(24) Salvador, P.; Hidalgo, M. G.; Zaban, A.; Bisquert, J. *J. Phys. Chem. B* **2005**, *109*, 15915–15926.
(25) Huang, S. Y.; Schlichthorl, G.; Nozik, A. J.; Grätzel, M.; Frank, A. J. *J. Phys. Chem. B* **1997**, *101*, 2576–2582.
(26) Jennings, J. R.; Wang, Q. *J. Phys. Chem. C* **2010**, *114*, 1715–1724.
(27) O'Regan, B. C.; Durrant, J. R. *Acc. Chem. Res.* **2009**, *42*, 1799–1808.
(28) Haque, S. A.; Palomares, E.; Cho, B. M.; Green, A. N. M.; Hirata, N.; Klug, D. R.; Durrant, J. R. *J. Am. Chem. Soc.* **2005**, *127*, 3456–3462.
(29) Heimer, T. A.; Heilweil, E. J.; Bignozzi, C. A.; Meyer, G. J. *J. Phys. Chem. A* **2000**, *104*, 4256–4262.
(30) Pelet, S.; Moser, J. E.; Grätzel, M. *J. Phys. Chem. B* **2000**, *104*, 1791–1795.
(31) Ruhle, S.; Cahen, D. *J. Phys. Chem. B* **2004**, *108*, 17946–17951.
(32) Kron, G.; Rau, U.; Werner, J. H. *J. Phys. Chem. B* **2003**, *107*, 13258–13261.
(33) Haque, S. A.; Tachibana, Y.; Klug, D. R.; Durrant, J. R. *J. Phys. Chem. B* **1998**, *102*, 1745–1749.

JP105486K